Romanian Reports in Physics **70**, 515 (2018)

TiO_2 2D NANOPATTERNS OBTAINED BY HIGH POWER IMPULSE MAGNETRON SPUTTERING DEPOSITIONS WITH COLLOIDAL MASKS

ALEXANDRA DEMETER, VASILE TIRON and LUCEL SIRGHI

Iasi Plasma Advanced Research Center (IPARC), Faculty of Physics, Alexandru Ioan Cuza University of Iasi, Iasi-700506, Romania
E-mail: *lsirghi@uaic.ro*

Received June 29, 2017

Abstract. Colloidal lithography was used to fabricate periodic 2D nanopatterns of TiO_2 on silicon substrate by two methods: a) reactive high power impulse magnetron sputtering (HiPIMS) deposition of TiO_2 on substrates with colloidal masks and mask lift-off; b) HiPIMS deposition of titanium on substrates with colloidal masks, mask lift-off and thermal oxidation. For the reactive deposition it was used multipulse HiPIMS (a single HiPIMS pulse was decomposed into a sequence of three shorter micropulses) of a pure Ti target in Ar and O_2 gas mixture. For the physical deposition of titanium, it was used HiPIMS of the same titanium target at the same power (100 W) in pure Ar gas. The Ti 2D patterns obtained by the latter method were thermally oxidized in oxygen atmosphere at 900°C for 2 h. The morphology of the fabricated TiO_2 patterns was investigated by atomic force microscopy (AFM) and scanning electron microscopy (SEM). The photocatalityc activity in visible light towards degradation of methylene blue dye molecules in aqueous solutions and UV light induced hydrophilicity of the fabricated 2D nanopatterned surfaces were investigated.

Key words: nanopatterned surfaces, colloidal lithography, photocatalytic activity, HiPIMS, TiO_2.

1. INTRODUCTION

Colloidal lithography (CL) is a powerful and cost-effective method of obtaining nanopatterns with controlled morphology over relatively large surface area. The CL technique uses the property of particles from a colloidal solution to self-assemble in close packed monolayers over a substrate to fabricate colloidal masks (CMs) that are used afterwards in deposition or etching processes to create patterned surfaces [1]. The self-assembly methods used for CM fabrication are diverse: dip-coating, floating on an interface, electrophoresis deposition, physical and chemical template-guided self-assembly, and spin-coating [2], the latter method being used in the present study. Spin-coating provides advantages of scaling up and mass production because the process is rapid and compatible with wafer processing. Compared with the conventional lithography methods, the CL is highly efficient in fabricating 2D patterned nanostructures over large areas because it is time-saving with low equipment

cost [3]. The 2D nanostructures fabricated by CL have attracted great attention because of the potential applications in technological fields such as biosensors, data storage and optoelectronic devices [4]. The advancement and development of these applications rely strongly on the design and controlled fabrication of nanoparticle arrays and patterned films. In particular, patterned metal films fabricated by depositions on substrates with CMs constitute periodic 2D structures with interesting plasmonic properties [5]. Moreover, thermal oxidation of such 2D metal nanopatterns may result in fabrication of metal oxide patterns with enhanced photocatalytic activity [6].

In this study we use particles of polystyrene self-assembled in a hexagonally close-packed array as colloidal masks and plasma assisted thin film depositions for fabrication of Ti and TiO_2 patterns on silicon substrates [1]. For the plasma assisted depositions, we use high power impulse magnetron sputtering (HiPIMS) of a pure Ti target in pure Ar or in Ar/O_2 to deposit thin films of Ti, respectively, TiO_2. The HiPIMS is a sputtering technique where pulses of high density power (> kW/cm^2) are applied to the magnetron target at low duty cycle and low repetition frequency, thus generating high-density plasma with highly ionized deposition flux and broad energy distribution function of the sputtered species [7]. The high ion-to-neutral ratio and intense energetic particle bombardment which takes place during HiPIMS process enables to growth ultra-dense and smooth thin films [8, 9] and make possible to tailor the phase composition, microstructure and morphology, elemental composition, and subsequently the properties and functionality of the deposited thin films [10–13]. In the reactive HiPIMS in Ar/O_2 gas mixture, the TiO_2 2D nanopatterns were obtained directly, while HiPIMS in Ar yields Ti patterns that were afterwards thermally oxidized to obtain TiO_2 patterns. The photocatalytic activity in visible light towards decomposition of organic dye molecules in aqueous solutions for the TiO_2 2D nanopatterns fabricated by the two HiPIMS operation modes is investigated.

2. PATTERN FABRICATION AND CHARACTERIZATION

2.1. MATERIALS AND METHODS

The following reagents were used in spin coating deposition of CMs: aqueous colloidal solutions of polystyrene (PS) (PS nanospheres with a diameter of 500 nm and concentration of 10 wt%) and ethanol (99.8 %) from Sigma Aldrich and deionized water (DW) (electric resistivity > 18 MΩ·cm) prepared by a Milli-Q filtering system (Super-Q® Plus System from Merk Millipore). A detailed description of CMs deposition process is given in [6].

The TiO_2 2D patterns were fabricated by two methods hereinafter referred to as M_1 and M_2. The method M_1 consists in CM deposition, followed by reactive HiPIMS deposition of a thin film of TiO_2 on the substrate with CM and mask lift-off. The method M_2 consists in CM deposition, followed by physical HiPIMS deposition of Ti, mask lift-off and thermal oxidation. The fabrication steps followed in each method are presented in Fig. 1. The left side of the figure presents the fabrication

steps of M_1, while the right side presents the fabrication steps of M_2. In M_1, the TiO_2 thin films (with thickness around 100 nm) were deposited on substrates with close packed CMs of polystyrene beads (500 nm in diameter) by reactive HiPIMS working in multi-pulse mode (m-HiPIMS). The thickness of the deposited thin films was measured *in-situ*, using a quartz crystal microbalance (QCM) placed near the port-substrate. The QCM measurements were calibrated by using the film thickness values determined from analysis of scanning electron microscopy images (not shown) of the deposited film cross sections. The magnetron was powered (the average power was around 100 W) by a high power pulse generator with the pre-ionization voltage set to maintain a constant discharge current intensity of about 8 mA between pulses or pulse sequences. In the case of m-HiPIMS deposition, sequences of three high voltage (-950 V) pulses with 3 μs in width and 50 μs in delay time were applied to the cathode with a repetition frequency of 600 Hz. The titanium target (99.95% Ti purity) with the diameter of 50 mm and thickness of 5 mm has been sputtered in Ar/O_2 gas mixture (mass flow rates of 50 sccm and 0.1 sccm, respectively) at the total pressure of 5 mTorr. The mass flow rates were controlled by two mass flow controllers (MKS Instruments, Inc), while the total gas pressure was adjusted by the opening of the valve separating the deposition chamber from the vacuum pumping system. The distance between the target and the substrate was 100 mm and the substrates were kept at the room temperature. For the physical HiPIMS deposition of titanium in M_2, we used the same deposition setup. The deposition runs were carried out by single-pulse HiPIMS of the same Ti target in pure Ar at constant average power (100 W) and target-substrate distance (100 mm). The mass flow rate and pressure of Ar were kept constant at 10 sccm and 3 mTorr, respectively. Ultra-short voltage pulses (5 μs duration) with amplitude of –1 kV were applied to the magnetron cathode to determine high power discharge pulses with peak values of the current intensity around 30 A. Details on the experimental set-up and HiPIMS technique can be found in a previous work [14].

After the depositions (reactive and metallic), the colloidal masks with the deposited films on their top were removed by sonication in DW water for 3 minutes. This left the 2D nanopatterns of TiO_2 or Ti on the silicon substrates. In M_2 an additional fabrication step is necessary to obtain the TiO_2 nanopatterns. In this step, the silicon substrates with the Ti 2D nanopatterns were thermally oxidised at 900°C in oxygen gas at atmospheric pressure for 2 h. The oxidation was performed in the same chamber (used also in nanopaterns depositions) vacuumed at 1×10^{-7} Torr and filled with pure oxygen (purity of 99.999%) at atmospheric pressure.

The photocatalytic activity of the TiO_2 2D patterns was characterized by measuring the degradation rate of methylene blue (MB) dye in aqueous solution (initial concentration of 440 ppm) under visible light irradiation. The hydrophilic property of nanopatterned surfaces was evaluated by measuring the static water contact angle in ambient air atmosphere using the sessile-drop method. The lateral images of sessile water droplets were acquired by a digital microscope and analyzed by ImageJ software using ellipse approximation of the droplet profiles.

2.2. MICROSCOPY ANALYSIS OF PATTERN MORPHOLOGY

The surface topography of the fabricated TiO_2 patterns was investigated by an atomic force microscope (XE70 from Park System, South Korea) operated in tapping mode with a silicon AFM probe (HQ: NSC35/NoAl from μmasch) with tip curvature radius of 10 nm (nominal value) and cantilever frequency of 388 KHz.

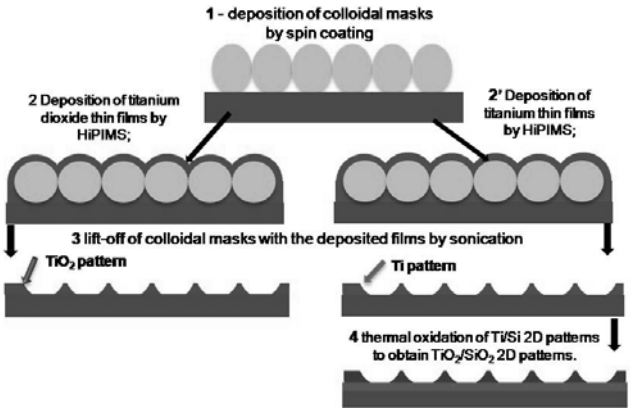

Fig. 1 – Schematic diagram of TiO_2 nano-pattern fabrication by plasma colloidal lithography using the method M_1 (left side: deposition of CM, reactive m-HiPIMS deposition of TiO_2 thin films, and mask lift-off), and the method M_2 (right side: deposition of CM, HiPIMS deposition of Ti, mask lift-off and thermal oxidation).

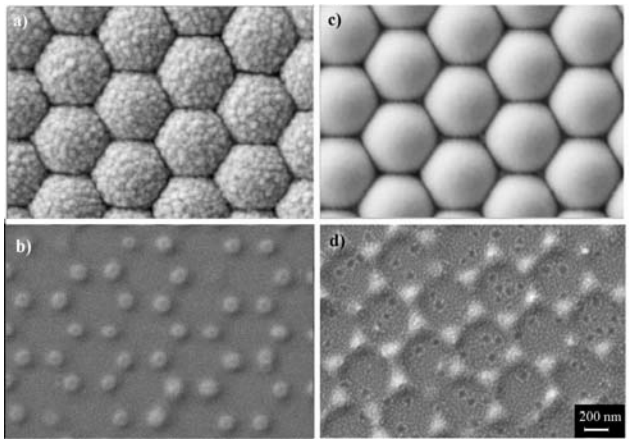

Fig. 2 – a) SEM image of TiO_2 thin film (thickness around 100 nm) deposited on the colloidal mask of PS beads with diameter of 500 nm; b) SEM image of TiO_2 nano-pattern (brighter area) remained on the silicon substrate (darker area) after lift-off of the colloidal mask; c) SEM image of the titanium film (thickness 60 nm) deposited by physical HiPIMS on the colloidal mask of PS beads with diameter of 500 nm; d) SEM image of Ti nano-pattern (brighter area) remained on the silicon substrate (darker area) after lift-off of the colloidal mask. The scale indicated by the white bar (200 nm) is same for all images.

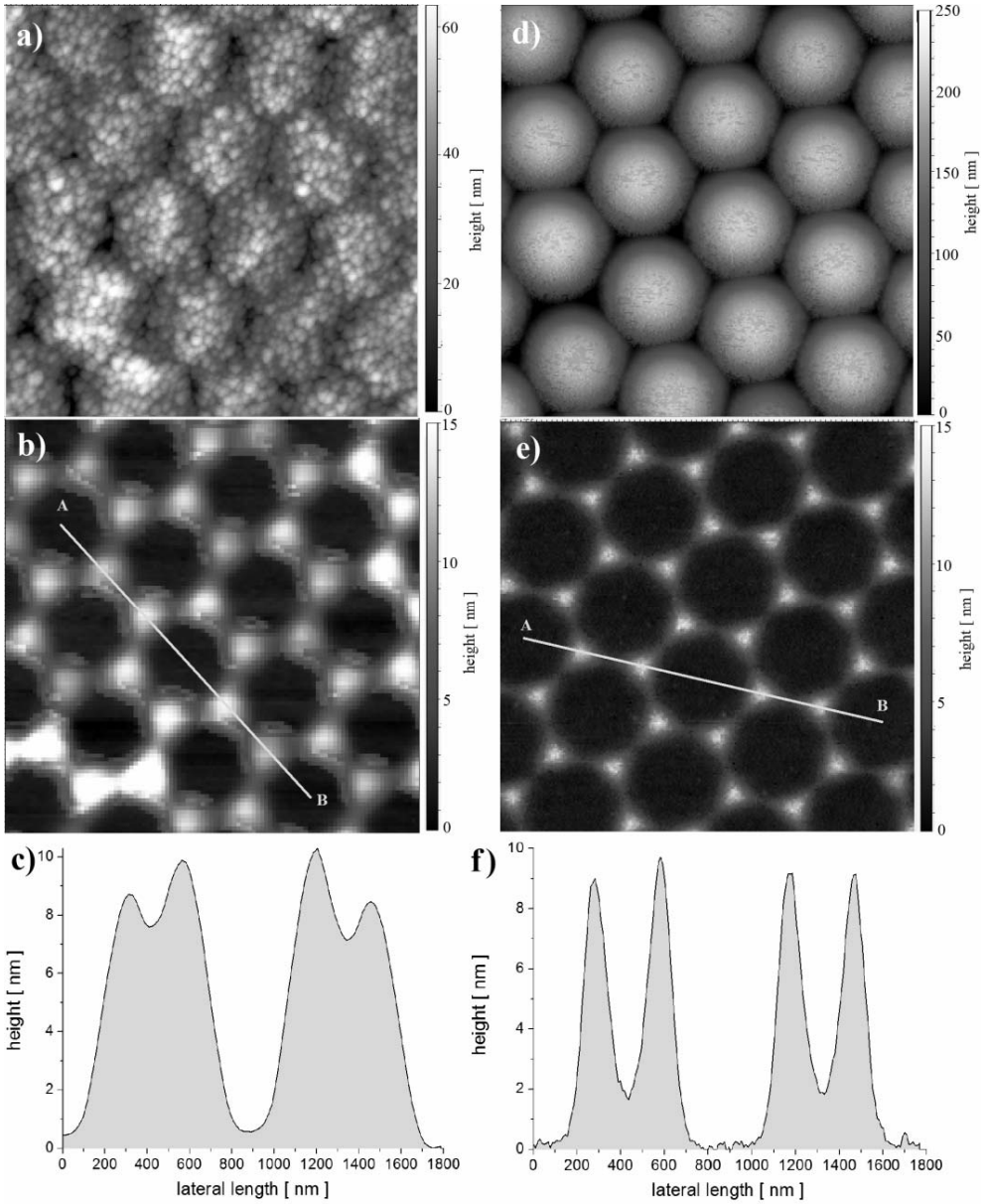

Fig. 3 – a) AFM topography image (scanned area 2 μm × 2 μm) of the colloidal mask covered by a titanium dioxide thin film deposited by reactive m-HiPIMS; b) AFM topography image of TiO_2 nano-pattern fabricated by M_1; c) height profile of the TiO_2 pattern along the pattern symmetry line (AB) shown on the panel b; d) AFM topography image of the colloidal mask covered by a titanium thin film deposited by HiPIMS; e) AFM topography image of Ti nano-pattern fabricated by HiPIMS deposition and mask lift-off steps in M_2; f) height profile of the Ti pattern along the pattern symmetry line (AB) shown on the panel e.

The topography images were levelled by in house software in order to correctly distinguish the TiO_2 structures on the flat substrate.

Scanning electron microscopy (SEM) analysis was also used to investigate the morphology of the deposited TiO_2 patterns. The SEM system used in the study was Carl Zeiss Crossbeam Neon 40ESB FIB. Scanning electron microscope images are shown in Fig. 2 to demonstrate the result of fabrication steps 2 in M_1, step 2' in M_2 and step 3 in both methods, as these fabrication steps were defined in Fig. 1. The SEM image in the panel a) shows a monolayer of self-assembled PS spheres coated with the TiO_2 film, which exhibits a rough surface. The spaces between the spheres are partially filled by TiO_2 as a result of the film growth. The sample surface after the removal of the PS nanospheres with the deposited film is shown in panel b). An hexagonal lattice of merged TiO_2 islands are visible (bright field) on the silicon substrate (dark field). The shape of the TiO_2 islands might be distorted by electrical charging o the TiO_2 material. The panel c) shows the SEM image of a monolayer of self-assembled PS spheres coated with a thin layer of Ti (around 60 nm in thickness). In this case, the film is more conform to the geometry of the substrate with CM (spherical shape of the beads underneath) and its surface is much smoother. The opening spaces of the CM are not completely filled by the film. The SEM image of the Ti 2D nanopattern resulted after lift-off of the mask with the film on top is presented in panel d). Because the value of Ar pressure used in deposition was low, the deposition flux of sputtered material in this case is anisotropic [6], fact that determined growing of well-defined Ti nanopatterns on the substrate places left unmasked by the colloidal mask.

The fabricated nano-patterns were also investigated by AFM to characterize their geometry and quality. The advantage of AFM analysis is that the sample surface topography is obtained in the real 3D space. To remove the AFM tip-sample convolution effects, the AFM images were deconvoluted by inverse tip image method [15]. Thus, the height profiles of patterns along certain directions can be obtained and analyzed. Figure 3 presents topography images of CM with deposited TiO_2 (panel a)) and Ti (panel d)) films and the corresponding 2D nanopatterns obtained after lift-off (panels b) and e)). The AFM images confirm the SEM images and show the morphology of the fabricated patterns in 3D space. The height of patterns was about 10 nm in both cases, but the TiO_2 pattern is bulkier, the triangular islands being merged in a hexagonal network. For the Ti pattern, the merging of the islands is less pronounced due to anisotropy of the deposition. These features are clearly visible on the height profiles of the patterns along a symmetry line (segments AB figured on the images). The height profiles show at island merging region a height about 8 nm for the TiO_2 pattern and about 2 nm for the Ti pattern. After the oxidation of Ti patterns, the height of resulted TiO_2 patterns increased to about 16 nm, and these results are consistent with those reported in reference [6].

2.3. HYDROPHILICITY AND PHOTOCATALYTIC ACTIVITY OF TITANIUM DIOXIDE 2D TITANIUM PATTERNS

Titanium dioxide is well known as a semiconductor with high photocatalytic activity under UV light irradiation. It is also known that the different features of the TiO_2 photocatalyst, such as the specific surface area, particle size, crystalline structure and stoichiometry have an important influence on its photocatalytic activity [5]. Presently, particular attention is being paid to activation of titanium dioxide photocatalysts by visible light irradiation. Recently, it was found that TiO_2 2D nanopatterns obtained by CL present improved photocatalytic activity in the visible region [6]. In the present work, we investigate the visible-light photocatalytic activity of the fabricated patterns by experiments of photocatalytic decomposition of methylene blue (MB) molecules in an aqueous solution. The photocatalytic activity of the fabricated TiO_2 nanopatterns in UV is investigated by studying the hydrophilicity improvement of the patterned surfaces caused by UV irradiation.

The photo-induced hydrophilicity of TiO_2 nanopatterns under UV light irradiation was evaluated by water contact angle measurements (WCA). The measurements were conducted in ambient air (temperature 25°C, relative humidity 60%) by analysis the height profiles of small sessile droplets (1 μl) of deionized water dropped on the surface of the TiO_2 nanopatterns before and after various times of UV light irradiation. The probes were radiated by a UV lamp (TUV T8 from Philips) at a power density of 1.8 $mWcm^{-2}$. In Fig. 4 it is shows comparatively the variation of water contact angle the TiO_2 patterns obtained by methods M_1 and M_2. Before UV irradiation, the patterns and film surfaces showed little hydrophilicity due to surface contamination with hydrophobic airborne hydrocarbon molecules [16], the WCA values being around 90 degrees. As result of the UV irradiation, the WCA decreased quickly for both TiO_2 patterns. The UV light induced improvement of hydrophilicity was slightly faster for the patterns fabricates by the method M_2, than for the patterns fabricated by the method M_1, probably due to a slight difference in the initial contamination of the two patterns.

The photo-catalytic activity of the fabricated TiO_2 nanopatterns in visible light was evaluated by measurements of the photocatalytic degradation of the MB dye in water under visible light irradiation. The TiO_2 nanopatterns were irradiated with visible light ($\lambda > 400$ nm) at a constant power density of 60 $mWcm^{-2}$. The degradation of the MB dye was estimated by spectral absorption measurements based on the reduction of the MB absorption peak at 664 nm. The volumetric concentration of MB in water (ppm) was measured based on calibration of the absorbance peak to the concentration of the MB solution. The MB dye was used as model compound for evaluation of photocatalytic activity of TiO_2 nanopatterns towards organic molecule contaminants in water. Figure 5 illustrates the reduction of MB concentration under visible light exposure in the presence of the TiO_2 nanopatterns irradiated by visible light. The results show that the pattern produced by M_1 is more active than that

produced by M_2. The time variations of MB concentration during photocatalytic decomposition show that the decomposition rate is not constant during the experiment. Thus, for the TiO_2 pattern obtained by reactive HiPIMS deposition (method M_1) the relative rate of photocatalytic decomposition of MB molecules:

$$\eta = -\frac{\Delta c}{c \cdot \Delta t} 100 \tag{1}$$

showed a large value during the first 10 minutes (around $4\% \cdot \text{min}^{-1}$) and a smaller value (around $1.5\% \cdot \text{min}^{-1}$) afterwards. Here, η is the relative rate of MB decomposition in percent per minute, c, the concentration of MB solution and Δc, the variation of MB concentration in the time interval Δt. For the TiO_2 pattern obtained by HiPIMS deposition of titanium and thermal oxidation (method M_2) the relative rate of photocatalytic decomposition of MB molecules also decreased quickly (during the first 10 min) from the initial value of $2\% \cdot \text{min}^{-1}$ to about $0.8\% \cdot \text{min}^{-1}$ and then remained constant. The rapid decrease of MB decomposition rate at the beginning of photocatalytic decomposition experiment is own to partially deactivation of surface redox sites generated by the light irradiation. The experiments of photocatalytic decomposition of MB show that the patterns generated by reactive HiPIMS have a better photocatalytic activity in visible light than the patterns generated by physical HiPIMS deposition of titanium and thermal deposition. This difference in photocatalytic activity might be determined by the difference in the crystalline structure of the TiO_2 patterns fabricated by the two methods. The X-ray diffraction (XRD) patterns showed an amorphous structure for the TiO_2 thin films deposited by reactive HiPIMS (XRD patterns not shown) and a polycrystalline structure with rutile phase in the TiO_2 thin films obtained by HiPIMS deposition of titanium and thermal oxidation (XRD patterns shown in [6].

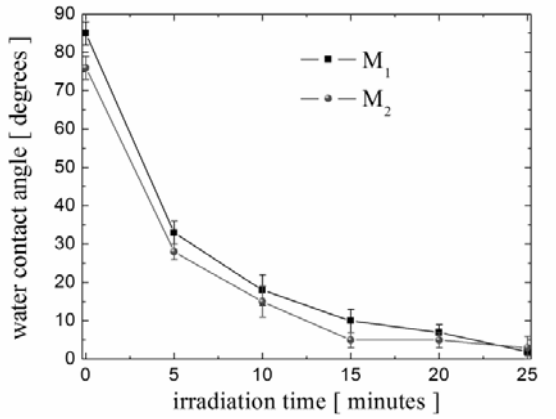

Fig. 4 – Variation of water contact angle for TiO_2 2D patterns obtained by the methods M_1 and M_2.

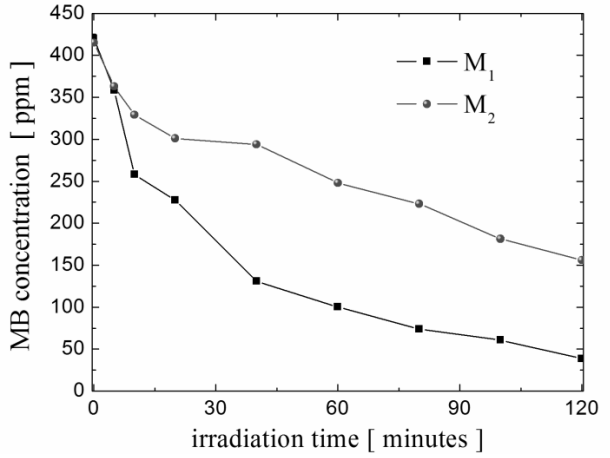

Fig. 5 – Variation of concentration of methylene blue (MB) aqueous solution as result of irradiation with visible light of TiO_2 patterns obtained by the methods M_1 and M_2.

3. CONCLUSION

High power impulse magnetron sputtering of a titanium target in Ar/O_2 and pure Ar gas was used to deposit TiO_2 and Ti, respectively, thin films on silicon substrates with colloidal masks consisting of close packed mono layers of polystyrene beads (500 nm in diameter). Lift-off by sonication in water of the masks with the deposited films on their top left highly ordered 2D patterns of TiO_2 or Ti on the substrates. The Ti patterns were thermally oxidized to finally obtain TiO_2 patterns. The morphology of the fabricated patterns was characterized by scanning electron microscopy and atomic force microscopy. Both investigation methods revealed highly ordered patterns with hexagonal symmetry inherited from the close packed colloidal masks. The height of both TiO_2 and Ti patterns was around 10 nm. The height of patterns increased after thermal oxidation to about 16 nm. The photocatalytic activity of the fabricated patterns was characterized by experiments of photocatalytic degradation of methylene blue molecules in water under visible light irradiation. These experiments showed that the patterns obtained by reactive HiPIMS deposition of TiO_2 have superior photocatalytic activity as compared to the patterns obtained by HiPIMS deposition of Ti and thermal oxidation. This difference might be caused by the difference in crystalline structure of TiO_2 in the fabricated patterns. The TiO_2 in patterns fabricated by reactive HiPIMS was amorphous while the TiO_2 in patterns fabricated by HiPIMS deposition of Ti and thermal oxidation presented polycrystalline rutile phase. The photocatalytic activity of the two patterns in UV light has been assessed by the improvement of surface hydrophilicity caused by UV light irradiation. Both patterns showed a quick improvement of surface hydrophilicity, their surfaces becoming super-hydrophilic after 25 minutes of UV light irradiation.

Acknowledgement. This work was supported by JOINT RESEARCH PROJECTS PN-II-ID-JRP-2012-RO-FR-0161.

REFERENCES

1. X. Ye, and L. Qi, Nano Today **6**, 608–631 (2011).
2. Y. Li, N. Koshizaki, and W. Cai, Coordin. Chem. Rev. **255**, 357–373 (2011).
3. A.K. Srivastava, S. Madhavi, T.J. White, and R.V. Ramanujan, J. Mater. Chem. **15**, 4424–4428 (2005).
4. M. Xu, N. Lu, H. Xu, D. Qi, Y. Wang, and L. Chi, Langmuir **25**, 11216–11220 (2009).
5. Y. Li, T. Sasaki, Y. Shimizu, and N. Koshizaki, J. Am. Chem. Soc. **130**, 14755–14762 (2008).
6. A. Demeter, V. Tiron, N. Lupu, G. Stoian, and L. Sirghi, Nanotechnology **28**, 255–302 (2017).
7. J.T. Gudmundsson, N. Brenning, D. Lundin, U. Helmersson, J. Vac. Sci. & Technol. A **30**, 030801 (2012).
8. M. Samuelsson, D. Lundin, J. Jensen, M.A. Raadu, J.T. Gudmundsson, and U. Helmersson, Surf. Coat. Technol. **205**, 591 (2010).
9. S. Konstantinidis, J.P. Dauchot, and M. Hecq, Thin Solid Films **515**, 1182 (2006).
10. K. Sarakinos, J. Alami, and S. Konstantinidis, Surf. Coat. Technol. **204**, 1661 (2010).
11. V. Tiron, I.-L. Velicu, M. Dobromir, A. Demeter, F. Samoila, C. Ursu, L. Sirghi, Thin Solid Films **603**, 255–261 (2016)
12. V. Tiron, L. Sirghi, Surf. Coat. Technol. **282**, 103–106 (2015).
13. V. Tiron, T. Coman, L. Sirghi, G. Popa, J. Optoelectron. Adv. M. **15**, 77–81 (2013).
14. O. Antonin, V. Tiron, C. Costin, G. Popa, T.M. Minea, J. Phys. D: Appl. Phys. **48**, 015202 (2015).
15. A.A Bukharaev, N.V. Berdunov, D.V. Ovchinnikov, and K.M. Salikhov, Scanning Microsc. **12**, 225–234 (1998).
16. A. Mills and M. Crow, Int. J. Photoenergy **2008**, 470670 (2008).